Annual carbon dioxide drawdown and the Northern Annular Mode

Joellen L. Russell
Atmospheric and Ocean Sciences, Princeton University, Princeton, New Jersey, USA

John M. Wallace
Department of Atmospheric Sciences, University of Washington, Seattle, Washington, USA

Received 28 January 2003; revised 5 August 2003; accepted 17 October 2003; published 28 January 2004.

[1] Year-to-year variations in summer drawdown of Northern Hemisphere atmospheric carbon dioxide (CO_2) are compared with corresponding year-to-year variations in sea-level pressure (SLP), surface air temperature, and the productivity of land vegetation as inferred from the satellite-derived normalized difference vegetation index (NDVI). Annual values of CO_2 drawdown for the years 1980–2000 are estimated from smoothed time series derived directly from individual flask samples at the nine Northern Hemisphere monitoring stations with the most continuous records. The leading principal component of the nine standardized drawdown time series, in which all stations exhibit positive loadings, is used to represent the hemispheric signal in the CO_2 drawdown. Linear regression analysis is used to infer the spatial patterns of anomalies in sea-level pressure, surface air temperature, and the NDVI observed during various seasons of years in which the drawdown is anomalously strong. Winters preceding anomalously high drawdown seasons exhibit patterns characteristic of the high index of the Northern Annular Mode (NAM). SLP tends to be anomalously low over the Arctic and high over midlatitudes, and Eurasia tends to be anomalously warm. The pattern of the NDVI observed during the early months of the growing season in years with anomalously high drawdown is indicative of high productivity over Eurasia. These results support the notion that the wintertime NAM influences the annual drawdown of CO_2 by modulating winter temperatures that, in turn, affect the productivity of the terrestrial biosphere during the subsequent growing season. *INDEX TERMS:* 0315 Atmospheric Composition and Structure: Biosphere/atmosphere interactions; 0330 Atmospheric Composition and Structure: Geochemical cycles; 1610 Global Change: Atmosphere (0315, 0325); 1615 Global Change: Biogeochemical processes (4805);
KEYWORDS: Arctic Oscillation, carbon dioxide, Northern Annular Mode

Citation: Russell, J. L., and J. M. Wallace (2004), Annual carbon dioxide drawdown and the Northern Annular Mode, *Global Biogeochem. Cycles*, *18*, GB1012, doi:10.1029/2003GB002044.

1. Introduction

[2] Records of atmospheric carbon dioxide exhibit a long-term upward trend largely due to the anthropogenic production of carbon dioxide (CO_2) through the burning of fossil fuels, which is moderated by the sequestration of carbon dioxide by the ocean through solubility, marine production, and, more speculatively, by the terrestrial biosphere [*Prentice et al.*, 2001].

[3] Superimposed upon this irregular upward trend is a seasonal cycle which is most pronounced over high latitudes of the Northern Hemisphere. Atmospheric CO_2 undergoes an abrupt decrease during the late spring months due to the excess of photosynthetic plant production over decay during the growing season and the more gradual recovery during the remainder of the year due to the continuing decay of the plant material produced during the growing season. The summer drawdown of CO_2 is largest and most abrupt over high latitudes of the Northern Hemisphere because the areal coverage of land is large, seasonal variations in insolation are large, and the growing season is concentrated in just a few months.

[4] The drawdown occurs dependably every year, as illustrated in Figure 1, but its magnitude varies in response to variations in the productivity of the high-latitude terrestrial biosphere. *Keeling et al.* [1996] reported a secular increase in the amplitude of the drawdown in the Mauna Loa record, which they attributed to increased productivity of Northern Hemisphere vegetation.

[5] Here we examine year-to-year variations in the magnitude of the drawdown and their relation to varying atmospheric circulation patterns over the Northern Hemisphere. Although ours is the first study to address this issue directly, there are several published studies of year-to-year variations in the productivity of Northern Hemisphere land vegetation and their relation to variations in the atmospheric circulation. Year-to-year variations in the width of the

0886-6236/04/2003GB002044$12.00

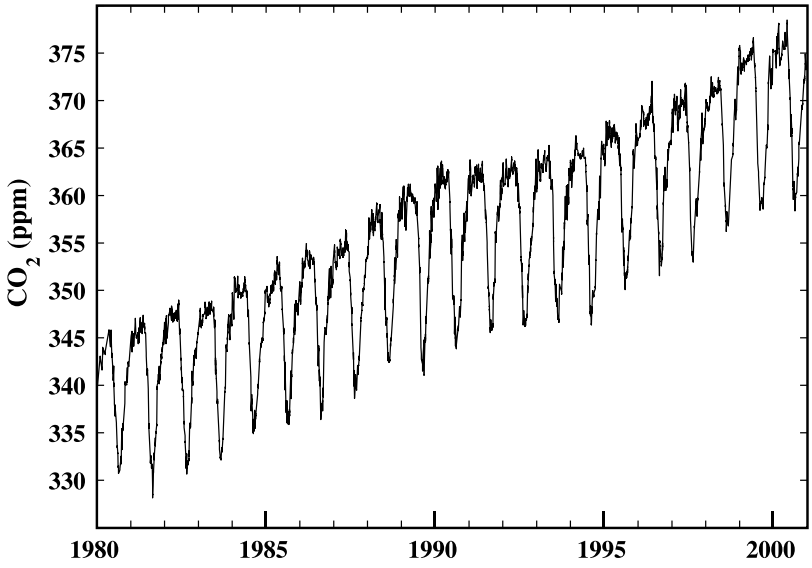

Figure 1. The 21-year record of the raw atmospheric carbon dioxide flask measurements at Barrow, Alaska.

annual growth rings of trees have been used with some success as a basis for constructing proxy indices of the primary mode of variability of the extratropical wintertime circulation (variously referred to as the North Atlantic Oscillation (NAO [*Hurrell*, 1995]), the Arctic Oscillation (AO [*Thompson and Wallace*, 1998]) and the Northern Hemisphere annular mode (NAM [*Hartmann et al.*, 2001])) during the previous winter [*Cook et al.*, 2002]. The so-called "high index" polarity of the NAO/AO/NAM (henceforth referred to as the NAM) is characterized by below-normal sea-level pressure over the Arctic centered near Iceland, above-normal pressure over midlatitudes with a prominent center over the Azores, and above-normal surface air temperatures over Eurasia and most of the United States. *Los et al.* [2001] and *Buermann et al.* [2003] have examined the greenness anomalies associated with this mode and found enhanced greenness over Eurasia accompanied by reduced greenness over high latitudes of North America.

[6] Our study is based on 21 years (1980–2000) of raw flask-derived atmospheric carbon dioxide data reported by the National Oceanic Atmospheric Administration's (NOAA) Climate Monitoring Diagnostics Laboratory (CMDL) Carbon Cycle Group. The drawdown is defined by the difference between the peak value observed within 2 months of the start of the growing season and the depth of the pronounced dip that is observed around the end of the growing season. In view of the relatively short timescale for regional anomalies in a passive tracer like CO_2 to be mixed throughout the hemisphere, we expect that such a signal should be of the same polarity at all stations; that is, apart from sampling variability, all stations should exhibit anomalously large and small summer drawdowns during the same sets of years. In the following section, we show evidence of the existence of such a hemispheric signal that is evident, to varying degrees, in data from the nine Northern Hemisphere monitoring stations that have the most complete records of observations during the 21-year period 1980–2000.

[7] In section 3 we attempt to relate the time series of CO_2 drawdown to spatially coherent variations of the hemispheric circulation, as expressed in the sea-level pressure field, during the season in which the drawdown is taking place, and during preceding and subsequent seasons as well. The analysis is based on sea-level pressure and surface air temperature from the NOAA NCEP/NCAR reanalysis [*Kalnay et al.*, 1996] for the same 21-year period.

[8] As in previous studies of the greenness of the terrestrial biosphere, we represent the greenness of the terrestrial biosphere by the NDVI, derived from the NOAA's Advanced Very High Resolution Radiometer (AVHRR). The radiometers measure emitted and reflected radiation in one visible, one near, and one middle infrared, and two thermal channels. The NDVI is calculated from the visible and near-infrared bands. The vegetation index exploits the property of green, vigorous vegetation to reflect strongly in the infrared band while at the same time strongly absorbing in the red band. Accordingly, the NDVI is commonly referred to as "greenness." The NDVI data are strongly correlated with terrestrial net primary production (NPP) and are frequently used as proxies of NPP [*Field et al.*, 1995; *Prince and Goward*, 1995]. It must be noted that the correlation between the satellite-derived NDVI and the actual NPP on the ground will vary according to biome and season [*Gamon et al.*, 1995; *Kicklighter et al.*, 1999]. There are also possible discontinuities in the NDVI due to the compilation of separate satellite missions [*Gutman and Ignatov*, 1995], but the 20-year record and complete global coverage make the NDVI the best available direct proxy for global terrestrial vegetation [*Tucker et al.*, 1986; *Keeling et al.*, 1996; *Hunt et al.*, 1996; *Myneni et al.*, 1997, 1998]. In the final section

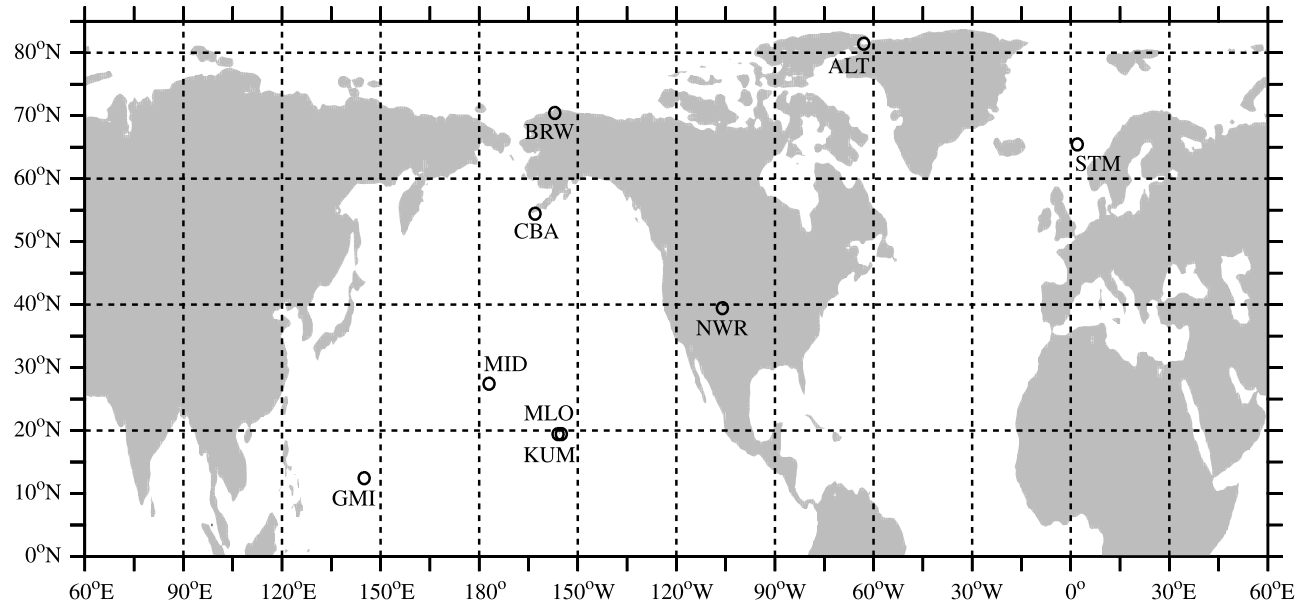

Figure 2. Locations of the nine stations used in this study.

of the paper, we present a brief summary and interpretation of the results.

2. Isolation of the Hemispheric Drawdown Signal

[9] We began by examining the records of the 13 longest-running Northern Hemisphere stations. We took the raw flask data for each station and calculated the daily average for each day with observations, removing all measurements flagged by CMDL as unacceptable. We then calculated a 30-day centered mean over of the daily flask data at each station for each of the 7665 days in the 21-year record (leap days are ignored so that each year is 365 days). Dates more than 30 days removed from the nearest flask observation were flagged as having missing data. All of the smoothed station data were then analyzed for internal record gaps more than 30 days in length: four of the stations (Christmas Island (CHR), Key Biscayne (KEY), Ragged Point, Barbados (RPB), and Shemya Island (SHM)) had more than 10 gaps of 30 days or longer and more than 5 gaps of 40 days or longer. These stations were discarded, leaving the nine most continuous Northern Hemisphere records: Alert (ALT), Barrow (BRW), Cold Bay (CBA), Guam (GMI), Kumukahi (KUM), Midway (MID), Mauna Loa (MLO), Niwot Ridge (NWR), and Station M (STM), whose locations are shown in Figure 2.

[10] The annual CO_2 drawdown at each station was estimated from the 30-day running mean time series, rather than from the monthly mean data calculated at CMDL, which are based on a spline fit to the flask data (Figure 3). The differences are substantial, especially when the sharp dip in the CO_2 time series that marks the end of the summer drawdown occurs near the beginning or end of a calendar month. In such cases, the dips tend to be more pronounced, and consequently the drawdown tends to be larger in our calculations than in the monthly CMDL data.

[11] The drawdown time series for each station was standardized by removing the time mean and dividing by the standard deviation. For the stations with records shorter than 21 years (e.g., ALT and MID), the station mean drawdown was substituted in the years with missing data. The drawdown time series for each station are shown in Figure 4 and the correlation matrix between the station time series is shown in Table 1.

[12] The fact that many of the correlations listed in the table are low and some are even negative reflects the large sampling variability inherent in the drawdown time series, but the prevalence of positive correlations supports the notion of a spatially coherent, hemispheric signal. As an index of this signal, we use the leading principal component (PC) of the correlation matrix, which accounts for 36% of the combined variance of the nine standardized time series (compared to 20% for the second component). The loadings of the various stations in the corresponding leading empirical orthogonal function are shown in Figure 4. Since the loadings are all of the same sign, this index is indicative of hemisphere-wide year-to-year variations in summer drawdown. To verify that it is not merely a manifestation of sampling variability, we performed the same PC analysis on a pseudo-randomized data set created by reversing the order (in time) of four of the nine station time series in the matrix of input data. Out of the possible 126 combinations that are possible with nine stations, only five exhibited a leading PC that explains as large a fraction of the total variance as that of the original (unrandomized) data. In the following section the leading PC of these nine station time series (the top curve in Figure 4) is used as an index to represent the annual summer drawdown of CO_2 over the Northern Hemisphere.

3. Regression Analysis

[13] In this section, time-varying spatial fields of climatic variables are regressed on the standardized leading PC of

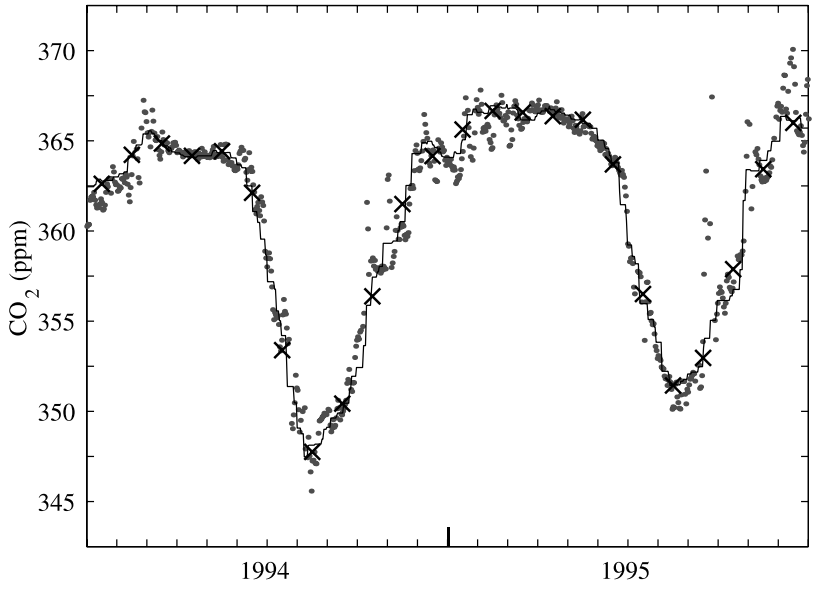

Figure 3. Comparison of the Barrow data as represented in three different formats. Light shaded dots are the individual daily observations, crosses are the monthly means derived from them, and the solid line represents the running 30-day mean smoothed data used in this analysis to represent the summer drawdown.

the drawdown time series, hereinafter referred to as the "reference time series." A regression coefficient R_n at the nth grid point in the field is computed from the formula

$$R_n = \overline{x'_n \cdot y'},$$

where x is the time series of the climatic variable at the nth grid point, y is the standardized reference time series, the overbar represents a time average over the 21-year record and the primes represent a deviation from the time average. In other words, R_n is simply the temporal covariance between x_n and y. The resulting "regression maps" (i.e., maps of the regression coefficients) represent the spatial patterns of the anomalies in the climatic variables that tend to occur during years in which the drawdown is larger than the 21-year average. They can be interpreted as weighted averages of the anomaly maps for all 21 years in which each year is assigned a weight in proportional to the anomaly in the drawdown for that year: years with drawdowns larger than the 21-year average are assigned positive weights, and years with smaller drawdowns are assigned negative weights, and the sum of the weights is equal to zero. Since the reference time series is standardized, contours on regression maps have the same units as the field that is being regressed. The amplitudes shown in regression maps of, say, sea-level pressure are indicative of the anomalies that occur in association with unit standard deviation in the reference time series and can thus be considered typical amplitudes.

[14] Regression maps are closely related to correlation maps. The zero contours on the two kinds of maps are identical, and the patterns are usually similar. At each point on the maps the regression coefficient R_n is equal to the correlation coefficient r_n times the temporal standard devi-

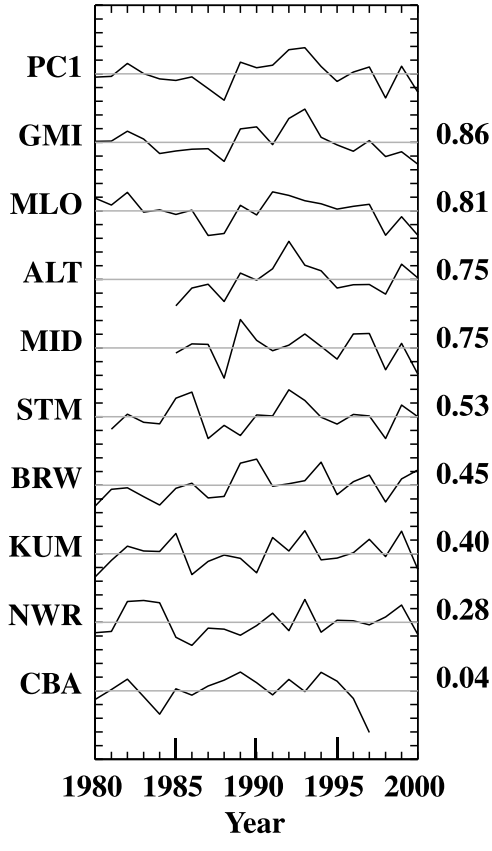

Figure 4. Standardized drawdown time series for the nine CMDL monitoring stations retained in this analysis and the leading principal component derived from them, as indicated. The weighting of each station in the leading principal component is listed at the right.

Table 1. Correlation Coefficients ($\times 10^{-2}$) for the CO_2 Drawdown Records (1980–2000) From Nine Northern Hemisphere Monitoring Stations[a]

BRW	STM	CBA	NWR	MID	MLO	KUM	GMI	
38	35	18	30	40	55	17	64	ALT
	24	29	−27	50	14	−02	35	BRW
		−07	−08	17	44	29	32	STM
			−22	−22	−09	−23	25	CBA
				09	20	57	21	NWR
					63	19	66	MID
						25	65	MLO
							18	KUM

[a]Records from stations like Guam and Alert are strongly correlated with the records from other stations.

ation of the grid point values of the field that is being regressed, i.e.,

$$R_n = r_n \sqrt{\left(\overline{x'^2}\right)}.$$

Because they contain amplitude information, regression maps provide a clearer indication of the actual patterns in a climatic field observed in association with variations in the reference time series than correlation maps do. Note that in contrast to the extrema on correlation maps, the peak values on a regression map may exceed unity.

[15] The regression maps shown in this section are based on consecutive 3-month means of climatic variables. We examined the entire suite of maps generated by regression 3-month means on the drawdown time series, starting with October/November/December of the preceding year, stepping forward 1 month at a time, and ending with July/August/September of the year of the drawdown, a total of nine sets of maps. We found the regression patterns to be strongest for the 3-month, ''late winter season'' January/February/March (JFM) and the correlation patterns for that season (not shown) to be nearly as strong as those for the growing season itself. Furthermore, we found some tendency for the climatic patterns set up during JFM to persist into the early months of the growing season (Figure 5).

[16] The JFM regression pattern, shown in Figure 6a, is characterized by below-normal surface pressure over the polar cap region and above-normal pressure at temperate latitudes. The strong meridional pressure gradient along the nodal line is indicative of enhanced westerly surface winds at subpolar latitudes. This pattern bears a remarkably strong resemblance to the leading EOF of the monthly mean SLP field poleward of 20°N for the same three calendar months and the same 21-year data set, shown in Figure 6b. The latter pattern is the basis for the definition of the NAM. The polarity of the patterns in Figure 6 (i.e., the fact that the center over the Arctic appears with a negative, rather than a positive algebraic sign) is consistent with the ''high index'' polarity of the NAM, as defined in section 1.

[17] A strong regression pattern may be indicative of a strong relation between the regressed field and the reference time series. On the other hand, it might be merely an indication of strong fluctuations in the climatic field that are only weakly correlated with the variations in the reference time series. Hence regression patterns need to be tested for statistical significance. The corresponding correlation patterns are often helpful in assessing the statistical

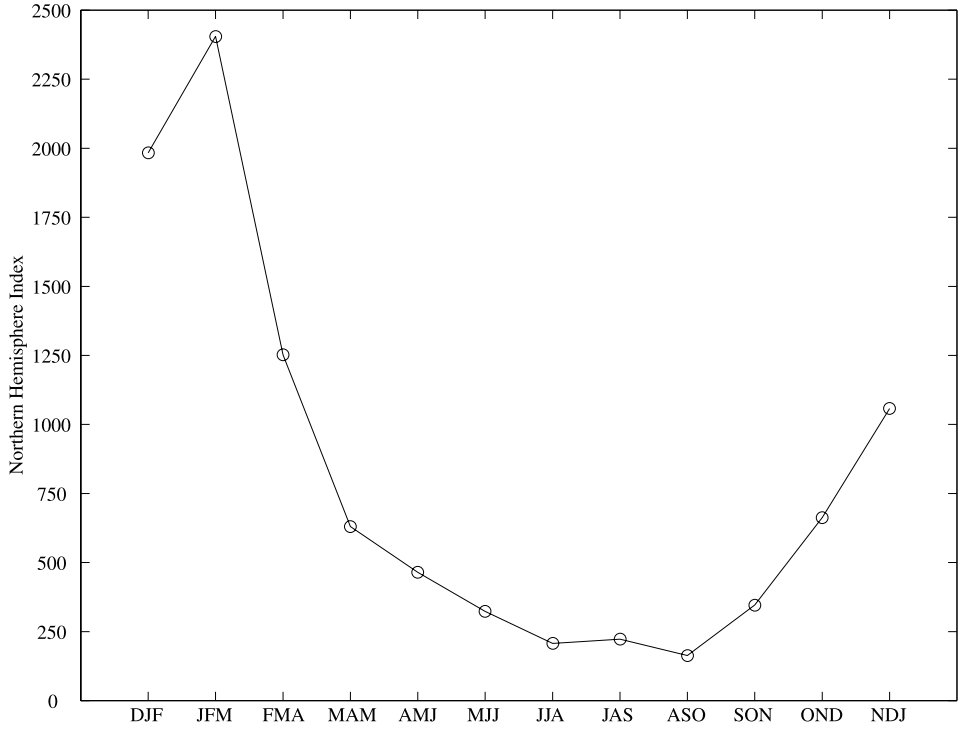

Figure 5. Total of the cosine-latitude-weighted covariance between the first mode of the CO_2 drawdown and the 3-month averaged NCEP SLP between 20°N and 90°N.

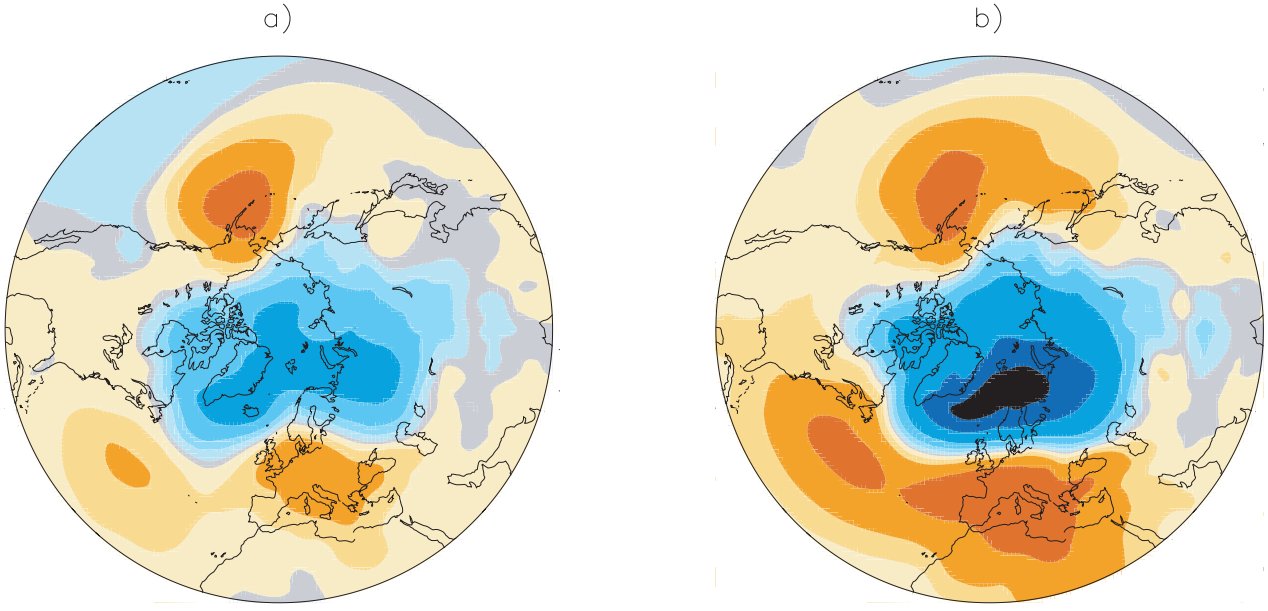

Figure 6. (a) Sea-level pressure (SLP) field averaged over the months January–March (JFM) regressed upon the standardized leading principal component (PC) of the annual drawdown of CO_2 during the growing season. (b) The JFM SLP field regressed upon the NAM-index as defined by the leading PC of monthly mean JFM SLP poleward of 20°N. Both patterns are based on the 21-year period of record 1980–2000. Contours are at (−6, −4, −2, −1, −0.5, −0.1, 0.1, 0.5, 1, 2, 4, 6) hPa; warm colors indicate positive anomalies; blue shades indicate negative anomalies; gray is straddling zero.

significance of regression patterns, but in order to interpret them it is necessary to understand the distinction between the "field significance" of a spatial pattern and the significance of correlations at individual grid points [*Livezey and Chen*, 1983]. Here, in lieu of presenting correlation maps, we apply two significance tests: one that focuses on the strength of the pattern and one that focuses on its resemblance to the NAM.

[18] To test the strength of the pattern in Figure 6a, irrespective of its relationship to the NAM, we compared it with 10,000 spatial patterns generated by regressing the same JFM SLP gridded data upon randomly generated, standardized time series of the same length, with the same 1-year lag autocorrelation as the drawdown time series (0.214). For each map, we computed the hemispheric mean (poleward of 20°N) of the area-weighted squared covariance (i.e., the square of the regression coefficient). The actual CO_2 drawdown time series had a higher average squared covariance than 92.2% of the randomly generated time series. To test the strength of the relationship with the NAM, we performed a t-test on the correlation coefficient between the leading PC of the drawdown and the leading PC of the SLP field, taking into account the autocorrelation inherent in the drawdown time series in estimating the degrees of freedom, using the formula of *Leith* [1971]. The observed correlation (0.55) is significant at the 95.5% level based on a two-sided test.

[19] The corresponding regression map for JFM surface air temperature (SAT) upon the standardized summer drawdown time series is shown in Figure 7a, from which it is evident that years with high summer drawdown tend to be preceded by above normal SAT over Eurasia poleward of 40°N, and negative anomalies over Canada and Alaska. The SAT regression pattern bears a striking resemblance to the pattern obtained by regressing the JFM SAT field upon the leading principal component of monthly mean JFM SLP for this 21-year record (Figure 7b); i.e., for the high-index polarity of the NAM.

[20] The regression pattern for the NDVI averaged over the early part of the growing season April–June (AMJ) upon the standardized summer CO_2 drawdown time series, shown in Figure 8a, exhibits enhanced greenness over most of Eurasia and reduced greenness over eastern Canada. A very similar and slightly stronger pattern is obtained by regressing each year's AMJ NDVI upon the wintertime NAM-index (i.e., the seasonal mean JFM value of the leading PC of the monthly mean JFM SLP field), as shown in Figure 8b.

4. Discussion

[21] The manner in which the CO_2 data are processed to estimate the summer drawdown strongly impacts the strength of the relationships described in the previous section. When the analysis is performed on the leading PC based on the drawdown time series for all 13 monitoring stations, processed as described in section 2, the correlation coefficient between the leading PC of the summer drawdown and the NAM-index was significantly lower than reported above. When the monthly CO_2 data set compiled by CMDL is used in place of the smoothed daily time series (retaining all 13 stations), the correlation is weaker still, but

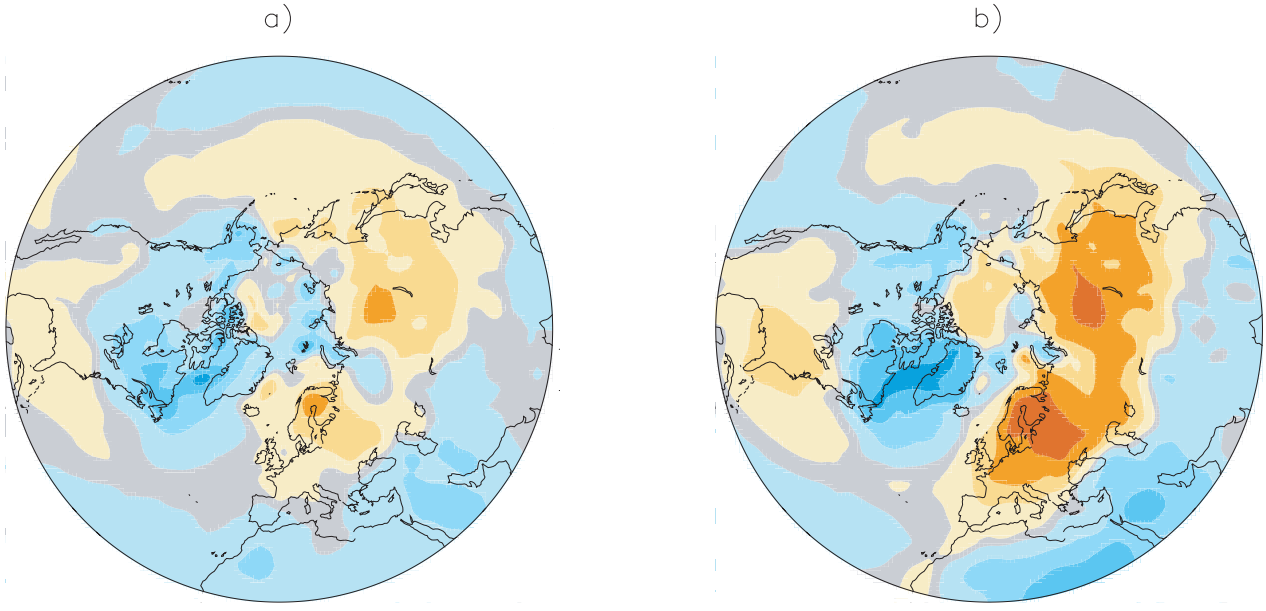

Figure 7. As in Figure 6 but for surface air temperature. Contours are at (−6, −4, −2, −1, −0.5, −0.1, 0.1, 0.5, 1, 2, 4, 6) °C; warm colors indicate positive anomalies; blue shades indicate negative anomalies; gray is straddling zero.

nonetheless suggestive of a relationship. In fact, it was just such an analysis that motivated this more careful examination of the summer drawdown. The NAM-related hemispheric signal in the drawdown time series is most clearly evident in the flask measurements at remote island stations Guam, Mauna Loa, and Midway in the subtropical Pacific. Regression patterns for those stations (not shown) are quite similar to those for the leading principal component of the drawdown time series. Had we not standardized the drawdown time series for individual stations before performing the principal component analysis, the first mode would have been dominated by the high-latitude continental stations, whose large day-to-day sampling variability renders them less representative of the hemisphere as a whole.

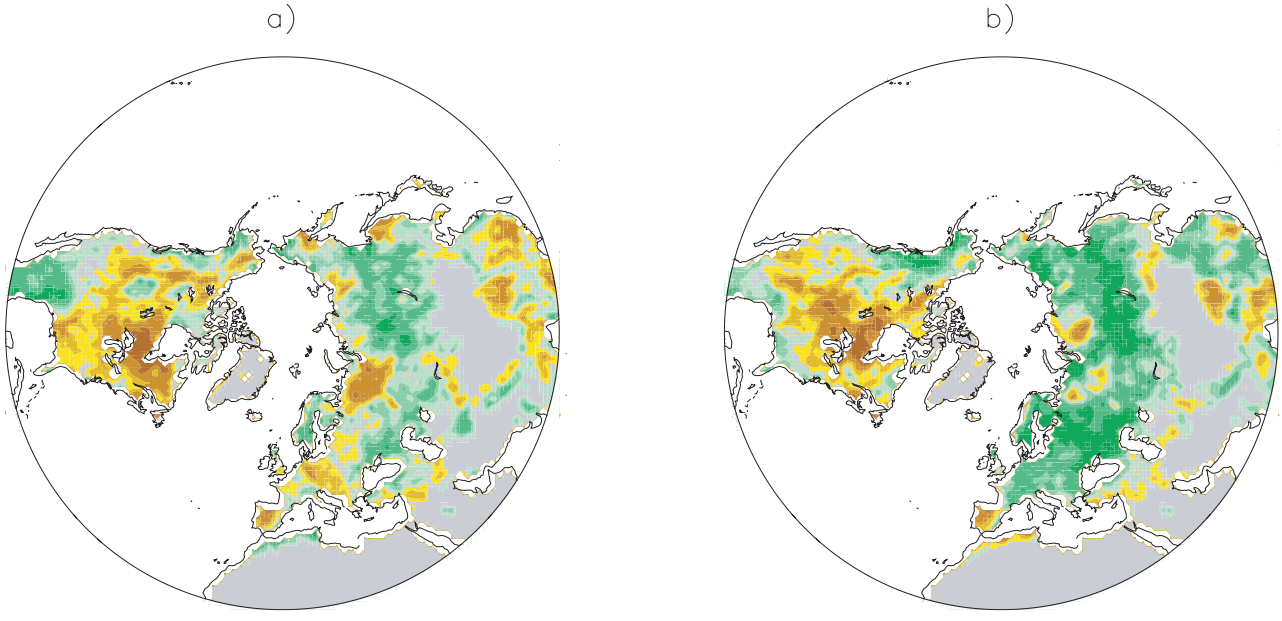

Figure 8. As in Figure 6 but for the NDVI averaged over April–June (AMJ). Green shades indicate enhanced greenness; yellows and browns indicate reduced greenness, gray is straddling zero. Contours are at (−6, −4, −2, −1, −0.5, −0.1, 0.1, 0.5, 1, 2, 4, 6) × 10^{-2} in dimensionless units.

[22] The regression patterns presented in the previous section that indicate a relationship between the wintertime NAM and the NDVI during the subsequent growing season are similar in many respects to results of *Buermann et al.* [2003] based on canonical correlation analysis between NDVI and surface air temperature and upper level geopotential height fields. The unique contribution of the present study is the documentation of the direct linear relationship between these fields and the summer drawdown in CO_2. Our analysis also demonstrates more clearly that the NAM-related signature in land vegetation is lagged by a season relative to the atmospheric circulation anomalies that presumably caused it.

[23] We considered the possibility that the correlation might merely be a reflection of a common trend in the NAM and drawdown time series. *Hurrell* [1995] and *Thompson et al.* [2000] have reported a trend toward the high index of the NAM. However, it is evident from a visual inspection of Figure 4 that the trend toward increasing summer drawdowns of CO_2 reported by *Keeling et al.* [1996] have not persisted through the period of our analysis. Hence the contribution of the common trend to the observed correlation between the wintertime NAM index and the summer drawdown is negligible. We also considered the possibility that the apparent influence of wintertime climate anomalies upon the drawdown during the subsequent growing season might merely be a reflection of the season-to-season autocorrelation of the NAM itself. Regression maps analogous to the one in Figure 7a, but for subsequent months (not shown), are, in fact, suggestive of some tendency for persistence of the wintertime NAM anomalies into spring, but the autocorrelation is not strong enough to explain the lag correlation between the wintertime NAM index and the summer drawdown. Hence we conclude that there must be a direct linkage.

[24] An anomalously large drawdown of atmospheric CO_2 following a high NAM-index winter could conceivably be a reflection of either enhanced productivity or suppressed respiration during the growing season. Given that wintertime respiration is small and that soil temperatures adjust to the ambient atmospheric temperatures and radiative fluxes within a period of days, it is difficult to imagine how wintertime temperature anomalies could affect respiration during the following summer. On the other hand, there are plausible mechanisms by which productivity could be influenced by antecedent climatic conditions. For example, the above-normal wintertime temperatures observed over Eurasia in association with the high index polarity of the NAM could result in less extensive snow cover in late winter, which would favor an anomalously early spring thaw, and an early start of the growing season. It is also worth considering whether there could be more direct biological processes whereby anomalously warm winter temperatures could promote increased productivity during the subsequent growing season.

[25] **Acknowledgments.** We wish to thank Todd Mitchell for helpful comments and assembly of some of the data sets used in this study. We thank Anjuli Bamzai for allowing us to use her unpublished calculations. We wish to thank Richard Feely for his advice and encouragement. We also wish to thank Pieter Tans for the most recent atmospheric carbon dioxide data. The NCEP/NCAR Reanalyses are made available by the NOAA-Climate Diagnostics Center (CDC). J. L. R. was supported by the Joint Institute for the Study of Ocean and Atmosphere (JISAO) under NOAA Cooperative Agreement NA67RJO155. J. M. W. was supported by the U.S. National Science Foundation under grant ATM 9707069. This is JISAO contribution 926.

References

Buermann, W., B. Anderson, C. J. Tucker, R. E. Dickinson, W. Lucht, C. S. Potter, and R. B. Myneni (2003), Interannual covariability in Northern Hemisphere air temperatures and greenness associated with El Niño-Southern Oscillation and the Arctic Oscillation, *J. Geophys. Res.*, *108*(D13), 4396, doi:10.1029/2002JD002630.

Cook, E. R., R. D. D'Arrigo, and M. E. Mann (2002), A well-verified, multiproxy reconstruction of the winter North Atlantic Oscillation index since AD 1400, *J. Clim.*, *15*, 1754–1764.

Field, C. B., J. T. Randerson, and C. M. Malmstrom (1995), Global net primary production—Combining ecology and remote-sensing, *Remote Sens. Environ.*, *51*, 74–88.

Gamon, J. A., et al. (1995), Relationships between NDVI, canopy structure, and photosynthesis in 3 Californian vegetation types, *Ecol. Appl.*, *5*, 28–41.

Gutman, G., and A. Ignatov (1995), Global land monitoring from AVHRR—Potential and limitations, *Int. J. Remote Sens.*, *16*, 2301–2309.

Hartmann, D. L., J. R. Holton, and Q. Fu (2001), The heat balance of the tropical tropopause, cirrus, and stratospheric dehydration, *Geophys. Res. Lett.*, *28*, 1969–1972.

Hunt, E. R., S. C. Piper, R. Nemani, C. D. Keeling, R. D. Otto, and S. W. Running (1996), Global net carbon exchange and intra-annual atmospheric CO_2 concentrations predicted by an ecosystem process model and three-dimensional atmospheric transport model, *Global Biogeochem. Cycles*, *10*, 431–456.

Hurrell, J. W. (1995), Decadal trends in the North Atlantic Oscillation region temperatures and precipitation, *Science*, *269*, 676–679.

Kalnay, E. M., et al. (1996), The NCEP/NCAR Reanalysis Project, *Bull. Am. Meteorol. Soc.*, *77*, 437–471.

Keeling, C. D., J. F. S. Chin, and T. P. Whorf (1996), Increased activity of northern vegetation inferred from atmospheric CO_2 measurements, *Nature*, *382*, 146–149.

Kicklighter, D. W., A. Bondeau, A. L. Schloss, J. Kaduk, and A. D. McGuire (1999), Comparing global models of terrestrial net primary productivity (NPP): Global pattern and differentiation by major biomes, *Global Change Biol.*, *5*, 16–24.

Leith, C. E. (1971), Atmospheric predictability and two-dimensional turbulence, *J. Atmos. Sci.*, *28*, 145–161.

Livezey, R. E., and W. Y. Chen (1983), Statistical field significance and its determination by Monte Carlo testing, *Mon. Weather Rev.*, *111*, 46–59.

Los, S. O., G. J. Collatz, L. Bounoua, P. J. Sellers, and C. J. Tucker (2001), Global interannual variations in sea surface temperature and land surface vegetation, air temperature, and precipitation, *J. Clim.*, *14*, 1535–1549.

Myneni, R. B., C. D. Keeling, C. J. Tucker, G. Asrar, and R. R. Nemani (1997), Increased plant growth in the northern high latitudes from 1981 to 1991, *Nature*, *386*, 698–702.

Myneni, R. B., C. J. Tucker, G. Asrar, and C. D. Keeling (1998), Interannual variations in satellite-sensed vegetation index data from 1981 to 1991, *J. Geophys Res.*, *103*, 6145–6160.

Prentice, C., G. D. Farquhar, M. J. R. Fasham, M. L. Goulden, M. Heimann, V. J. Jaramillo, H. S. Kheshgi, C. Le Quere, R. J. Scholes, and D. W. R. Wallace (2001), The carbon cycle and atmospheric carbon dioxide, in *Climate Change 2001*: *The Scientific Basis*, edited by J. Houghton et al., pp. 183–237, Cambridge Univ. Press, New York.

Prince, S. D., and S. N. Goward (1995), Global primary production: A remote sensing approach, *J. Biogeogr.*, *22*, 815–835.

Thompson, D. W. J., and J. M. Wallace (1998), The Arctic Oscillation signature in the wintertime geopotential height and temperature fields, *Geophys. Res. Lett.*, *25*, 1297–1300.

Thompson, D. W. J., J. M. Wallace, and G. C. Hegerl (2000), Annular modes in the extratropical circulation: II. Trends, *J. Clim.*, *13*, 1018–1036.

Tucker, C. J., I. Y. Fung, C. D. Keeling, and R. H. Gammon (1986), Relationship between atmospheric CO_2 variations and a satellite-derived vegetation index, *Nature*, *319*, 195–199.

J. L. Russell, Atmospheric and Oceanic Sciences, Princeton University, P.O. Box 308, Princeton, NJ 08542, USA. (jrussell@princeton.edu)

J. M. Wallace, Department of Atmospheric Sciences, University of Washington, P.O. Box 354235, Seattle, WA 98195-4235, USA. (wallace@atmos.washington.edu)